# Journal of Materials Chemistry C

Accepted Manuscript

This article can be cited before page numbers have been issued, to do this please use: Y. Jiao, M. Li, N. Wang, T. Lu, L. Zhou, Y. Huang, Z. Lu, D. Luo and X. Pu, *J. Mater. Chem. C*, 2016, DOI: 10.1039/C6TC00153J.

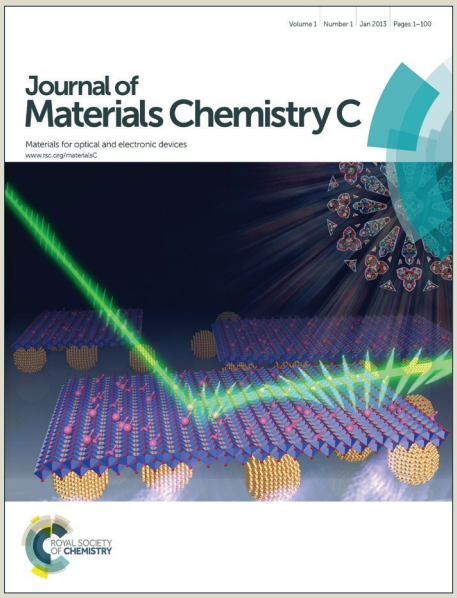




ROYAL SOCIETY OF CHEMISTRY

www.rsc.org/materialsC

View Article Online
DOI: 10.1039/C6TC00153J

Journal Name

ARTICLE

# A facile color-tuning strategy for constructing a library of Ir(III) complexes with fine-tuned phosphorescence from bluish green to red using synergetic substituent effect of –$OCH_3$ and –CN at merely the C-ring of C^N ligand

Received 00th January 20xx,
Accepted 00th January 20xx

DOI: 10.1039/x0xx00000x

www.rsc.org/

Yan Jiao,‡[a] Ming Li,‡[a] Ning Wang,[a] Tao Lu,[a] Liang Zhou,*[b] Yan Huang,[a] Zhiyun Lu,*[a] Daibing Luo[c] and Xuemei Pu*[a]

By simply grafting a –CN group and/or a –$OCH_3$ group on the *meta*- and/or *para*-site of the C-ring, a series of Ir(III) complexes bearing a similar molecular platform of bis(1,2-diphenyl-1*H*-benzimidazolato-*N*,$C^{2'}$)iridium(III)(acetylacetonate), but showing fine-tuned phosphorescence covering nearly the whole window of visible spectrum with a wide color-tuning range of 109 nm have been acquired. With the help of DFT calculations, it was unveiled that if the C-related arene moiety of the C^N ligand (C-ring) contributes substantially to both the HOMO and LUMO of an Ir(III) complex, the concurrent introduction of an electron-donating –$OCH_3$ and an electron-withdrawing –CN groups on the C-ring at the *meta*- and *para*-sites relative to Ir atom may lead to a favorable synergetic substituent effect on the color-tuning direction. This may represent a facile yet effective molecular design strategy for Ir(III) with desirous emission color. A bluish green organic light-emitting diode (OLED) based on one of the objective complex displays a maximum current efficiency of 62.1 cd $A^{-1}$, external quantum efficiency of 19.8%, and brightness of 48040 cd $m^{-2}$, implying that high-performance red and blue OLED phosphores as well as libraries of Ir(III) complexes bearing similar molecular platforms may be developed through this –$OCH_3$ and –CN synergetic substitution strategy.

## 1. Introduction

Recently, cyclometalated Ir(III) complexes have attracted considerable interests due to their potentials as luminogens in phosphorescent organic light-emitting diodes (PhOLEDs).[1] Although the performance of green Ir(III) complex-based PhOLEDs is satisfactory for practical applications,[2] there is still an urgent need for highly efficient red[3] and blue[4] PhOLED phosphores, so that high-performance full-color display devices could be achieved. As a consequence, the rational color-tuning of Ir(III) complexes over the entire visible region has emerged as an important task.[5]

Generally, the phosphorescence color of Ir(III) complexes could be fine-tuned through: 1) alteration of framework of the cyclometalated (C^N) ligand, since it is well-accepted that the emission color of an Ir(III) complex correlates highly with the conjugation length of its C^N ligand;[6] 2) modification of chemical structure of the ancillary ligand;[7] 3) grafting of substituent(s) at the C^N ligand while fixing the ligand skeleton.[5a] Nevertheless, it has been reported recently that the emission color of Ir(III) complexes do not always correspond to the extent of π-conjugation in their C^N ligand;[8] while the second strategy could work effectively only when the ancillary ligand contributes substantially to the frontier molecular orbitals (FMOs) of the complex.[7] Hence the substitution strategy might be a facile and straightforward way to understand the structure-properties relationship of Ir(III) complexes, through which rational molecular design of iridium complex with desirous emission color could be actualized. More importantly, through this strategy, a library of phosphorescent compounds bearing similar molecular platform but showing a wide color-tuning range could be easily constructed,[9] thereupon highly efficient energy-transfer luminogen pairs[10] could be achieved for further opto-electronic applications.[11]

Accordingly, many research efforts have been devoted to the fine-tuning of phosphorescence color of Ir(III) chelates through substituent effects, and the best understandable parent examples are $Ir(ppy)_2(acac)$ and $Ir(ppy)_3$ (Hppy = 2-phenylpyridine).[12] For $Ir^{III}$-ppy complexes, their HOMOs (highest occupied molecular orbital) were demonstrated to be located mainly on the Ir atoms and the C-related phenyl segments of their C^N ligands (denoted as C-ring here), but their LUMOs (lowest unoccupied molecular orbital) are primarily distributed on the N-related pyridine moieties (denoted as N-ring here).[13] Consequently, it is generally considered that the substitution of an electron-donating group (EDG) on the C-ring will induce

[a]*Key Laboratory of Green Chemistry and Technology (Ministry of Education), College of Chemistry, Sichuan University, Chengdu 610064, PR China*
**E-mail: xmpuscu@scu.edu.cn; Fax: +86-28-85412907. luzhiyun@scu.edu.cn; Fax: +86-28-85410059.*
[b]*State Key Laboratory of Rare Earth Resource Utilization, Changchun Institute of Applied Chemistry, Chinese Academy of Sciences, Changchun 130022, PR China*
**E-mail: zhoul@ciac.ac.cn.*
[c]*Analytical and Testing Centre, Sichuan University, Chengdu, 610064, PR China*
†Electronic Supplementary Information (ESI) available: [Synthetic procedures, characterization data, crystal data for **4d-4g**, theoretical calculation data, $^1$H NMR, $^{13}$C NMR, and HRMS spectra.]. See DOI: 10.1039/x0xx00000x
‡These authors contributed equally to this work.

View Article Online
DOI: 10.1039/C6TC00153J




raised HOMO level hence red-shifted emission of the complex; while the grafting of an electron-withdrawing group (EWG) on the C-ring will endow the complex with lowered HOMO level hence blue-shifted emission.[14] However, it has been unveiled recently that in addition to the electronic nature, the grafting position of a substituent at the C-ring would also have a strong influence on the color-tuning direction,[9,15-17] yet the tuning of phosphorescence color of Ir(III) complexes through substituent effects on the C-ring of C^N ligands still relies on certain serendipitous discoveries, and the relationship between emission color and electronic nature and position of substituent at the C-ring has not been well-elucidated.[9d,15] For example, despite the fact that the grafting of an EWG like trifluoromethyl on the C-ring at either the *meta*- or *para*-site relative to the Ir atom was found to induce a blue-shifted emission,[14a] in some cases, it was observed when pentafluorophenyl, carborane, sulfonyl, dimesitylboron or formyl was introduced to the *meta*-position (with respect to the Ir ion) of the C-ring, it would endow the complex with red- rather than blue-shifted emission, regardless of its EWG nature.[9b,9d,16] Similarly, although it has been demonstrated that the substitution of an EDG of diphenylamino on the C-ring at either the *meta*- or *para*-site relative to the Ir atom will result in red-shifted emission,[14b] in a few reports, it has been revealed that the introduction of an electron-donating $–OCH_3$ or $–CH_3$ group into the *meta*-site on the C-ring will endow the complex with blue-shifted rather than red-shifted phosphorescence.[9a,17] More recently, it was observed that the *para*-substitution of an EWG of dicyanovinyl at the C-ring will have negligible effect on the emission color of the complex; but its *meta*-grafting would lead to drastically red-shifted phosphorescence.[9d] Hence it is clear from the literature review that the rational molecular design of Ir(III) complexes with desirous emission color is still a challenge nowadays.[18]

In this work, we report our exciting discoveries that both the *meta*-grafting of a $–OCH_3$ and *para*-substitution of a –CN on the C-ring (with respect to the Ir atom) of bis(1,2-diphenyl-1*H*-benzimidazolato-*N*,$C^{2'}$)iridium(III)(acetylacetonate) would result in blue-shifted emission; while the *para*–$OCH_3$ and *meta*–CN substitution on the C-ring would both lead to red-shifted phosphorescence. It is noteworthy that the concurrent presence of a $–OCH_3$ and a –CN groups on the C-ring at *meta*- and *para*- sites will result in a favorable synergetic substituent effect on the color-tuning direction, leading to more red-shifted or blue-shifted emission. In fact, the simple alteration of the substitution position of $–OCH_3$ and –CN groups in the di-substituted complexes will result in a 109 nm color-tuning range, and all these $–OCH_3$ and –CN mono- and di-substituted complexes could comprise a library of Ir(III) complexes bearing similar molecular platform, but showing fine-tuned phosphorescence covering nearly the whole window of visible spectrum. More importantly, with the aid of density functional theory (DFT) calculations, the intrinsic reasons for the substituent effects of $–OCH_3$ and –CN groups on the color-tuning direction of Ir(III) complexes have been deciphered. Furthermore, electroluminescent (EL) characterization results revealed that PhOLEDs using these $–OCH_3$ and –CN di-substituted complexes as phosphore could display satisfactory EL performance, indicating that this simple color-tuning strategy should be quite effective to exploit diverse high-performance red and blue PhOLED Ir (III) complexes rationally.

## 2. Experimental

All experimental details including synthetic procedures of the intermediates and objective compounds, photophysical and electrochemical characterization, computation method as well as device preparation are given in the ESI.

## 3. Results and discussion

### 3.1. Molecular design, synthesis and characterization of the objective complexes

To achieve a molecular library of Ir(III) complexes capable of emitting phosphorescence covering the whole visible region, a high-performance green PhOLED phosphore, bis(1,2-diphenyl-1*H*-benzimidazolato-*N*,$C^{2'}$)iridium(III)(acetylacetonate) (**4a**),[19] was chosen as the parent compound. As the effect of a substituent on the aromatic system of a chelate is usually discussed in terms of both electronic (inductive and mesomeric) and steric effects (especially in case that two substituents were introduced into the *meta*- and *para*-sites concurrently), we chose $–OCH_3$, a small volume group showing just weak electron-withdrawing inductive but strong electron-donating mesomeric effects as the EDG, and –CN group, a small volume group showing both strong electron-withdrawing inductive and mesomeric effects as the EWG, so that the electronic effects of these substituents on the photophysical properties of the

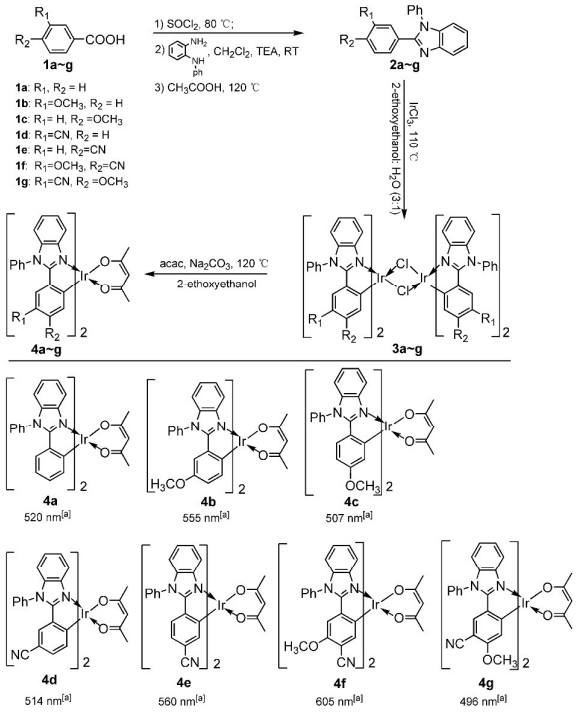


**Scheme 1.** The chemical structures and synthetic routes to the Ir(III) complexes **4a**~**4g**. For detailed synthetic procedures, see the supporting information. [a] PL emission maximum in dilute $CH_2Cl_2$ solution.

View Article Online
DOI: 10.1039/C6TC00153J





chelates could be clarified more straightforwardly.[18] The chemical structures of the parent complex **4a** and objective chelates **4b**~**4g** were shown in Scheme 1, and the detailed synthetic routes to these complexes are shown in Scheme S1.

The chemical structures of **4a**~**4g** were confirmed by $^{1}$H NMR, $^{13}$C NMR, and HRMS (ESI) spectrometry, and the molecular structures of **4d**, **4e**, **4f**, and **4g** were further confirmed *via* X-ray crystallography characterization. The ORTEP drawing of the crystal structures, crystallographic refinement parameters as well as selected bond length/angle of **4d**~**4g** were depicted in Figure S1 and Tables S1~S2.

### 3.2. Photophysical properties

The absorption spectra of **4a**~**4g** in dilute solutions ($5\times10^{-6}$ mol $L^{-1}$ in $CH_2Cl_2$) were displayed in Figure 1, and relevant data were summarized in Table 1. All these compounds exhibit two distinguishable absorption bands in UV-Vis region, *i.e.*, a stronger one with absorption maximum ($\lambda_{abs\ max}$) of 300~320 nm, and a weaker one with $\lambda_{abs\ max}$ of 390~460 nm. The former band at the higher-energy region is often assigned to the ligand-centered (LC) π-π transition of the C^N ligand; and the latter one at the lower-energy region is generally assigned to a mixed metal to ligand charge transfer (MLCT) and LC transition.[6a] Although **4a**~**4g** show analogous $\lambda_{abs\ max}$ in the higher-energy band, their $\lambda_{abs\ max}$ in the lower-energy one is quite dissimilar. In comparison with **4a** whose $\lambda_{abs\ max}$ = 412 nm, **4b** and **4e** bearing a *para*–OMe or *meta*–CN groups respectively both display bathochromic shift in this band with $\lambda_{abs\ max}$ of 430 nm; but the *meta*–OMe substituted **4c** and *para*–CN modified **4d** were both found to show slightly blue-shifted absorption with $\lambda_{abs\ max}$ of 405~409 nm. Excitingly, in the cases of the di-substituted **4f** and **4g**, their –$OCH_3$ and –CN groups show a synergistic substitution effect with regard to the fine-tuning of absorption bands of the complexes: for **4f** bearing not only a *para*–OMe but also a *meta*–CN group, its $\lambda_{abs\ max}$ locates at 458 nm, which is the most red-shifted one among all these complexes; while for **4g** bearing both *meta*–OMe and *para*–CN substituents, it shows the most blue-shifted $\lambda_{abs\ max}$ of 392 nm among **4b**~**4g**.

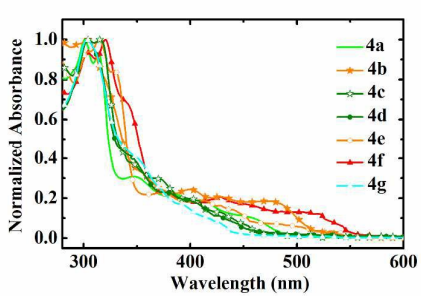


**Figure 1**. Normalized UV-Vis absorption spectra of **4a**~**4g** in dilute $CH_2Cl_2$ solutions.

Under photoexcitation, **4b**~**4g** emit intense room-temperature phosphorescence with structureless emission bands (vide Figure 2 and Table 1). Consistent with the optical bandgap data derived from absorption spectra, the *para*–$OCH_3$ (**4b**) or *meta*–CN (**4e**) modification would both lead to bathochromic shift of phosphorescence; the *meta*–$OCH_3$ (**4c**) or *para*–CN (**4d**) substitution would induce blue-shifted photoluminescence (PL) of the complex; while **4f** bearing not only a *para*–$OCH_3$ but also a *meta*–CN shows the most red-shifted PL among all these complexes ($\lambda_{em\ max}$ = 605 nm), **4g** bearing both a *meta*–$OCH_3$ and a *para*–CN displays the most blue-shifted PL emission band with $\lambda_{em\ max}$ of 496 nm. That is, for di-substituted **4f** and **4g**, their –$OCH_3$ and –CN groups also display a synergistic substituent effect on the tuning direction of emission color. It is noteworthy that this color-tuning strategy is quite effective, since the simple exchange of substitution positions of –$OCH_3$ and –CN in **4f** and **4g** would result in a 109 nm shift in the $\lambda_{em\ max}$. More excitingly, these –$OCH_3$ and/or –CN mono- or di-substituted compounds **4b**~**4g** constitute a molecular library bearing similar skeleton of **4a**, but showing phosphorescence covering nearly the whole visible spectrum region from bluish green to red.

In dilute solution, **4b**~**4g** display $\varphi_{PL}$ of 0.05~1.00. In comparison with **4a**, **4b**, **4e** and **4f** with red-shifted PL bands all show lower $\varphi_{PL}$; but **4c**, **4d** and **4g** with more hypochromic-shifted $\lambda_{em\ max}$ show comparable or higher $\varphi_{PL}$ of 0.91, 0.62 and 1.00 in sequence. When being blended into the host matrix of

**Table 1.** Photophysical, electrochemical, decomposition temperature, calculated frontier molecular orbital energy levels and energy gap data of **4a**~**4g**.

| Compd. | $\lambda_{abs\ max}$ [a] (nm) | $\lambda_{em\ max}$ [a] (nm) | $\varphi_{PL}$ [b] | $\varphi_{PL}$ [c] | $E_{1/2}^{ox}$ [d] (V) | HOMO [e] (eV) | LUMO [f] (eV) | $E_g$ [g] (eV) | $T_d$ [h] (°C) | CIE [i] (x, y) |
|---|---|---|---|---|---|---|---|---|---|---|
| **4a** | 300,315,348,385,412,458 | 520 | 0.64 | 0.16[j] | 0.34 | –5.14 (–5.03) | –2.73 (–1.29) | 2.41 (3.74) | 316 | (0.36,0.60)[j] |
| **4b** | 293,305,315,355,403,430,475 | 555 | 0.29 | 0.42 | 0.13 | –4.93 (–4.75) | –2.68 (–1.32) | 2.25 (3.43) | 294 | (0.50,0.50) |
| **4c** | 304,316,347,370,392,409,430 | 507 | 0.91 | 0.58 | 0.29 | –5.09 (–5.01) | –2.61 (–1.15) | 2.48 (3.86) | 318 | (0.30,0.60) |
| **4d** | 303,315,345,370,380,405,428 | 514 | 0.62 | 0.52 | 0.66 | –5.46 (–5.49) | –3.00 (–1.63) | 2.46 (3.86) | 365 | (0.32,0.61) |
| **4e** | 303,315,331,375,410,430,480 | 560 | 0.29 | 0.46 | 0.60 | –5.40 (–5.43) | –3.12 (–1.96) | 2.28 (3.47) | 389 | (0.50,0.49) |
| **4f** | 304,321,338,382,430,458,500 | 605 | 0.05 | 0.19 | 0.43 | –5.23 (–5.13) | –3.15 (–1.95) | 2.08 (3.18) | 335 | (0.65,0.35) |
| **4g** | 301,349,370,392,424 | 496 | 1.00 | 0.62 | 0.63 | –5.43 (–5.43) | –2.90 (–1.43) | 2.53 (4.00) | 313 | (0.27,0.57) |

[a] Measured in argon degassed $5\times10^{-6}$ mol $L^{-1}$ $CH_2Cl_2$ solutions; [b] relative PL quantum yields determined in argon degassed $5\times10^{-6}$ mol $L^{-1}$ $CH_2Cl_2$ solutions with *fac*-Ir(ppy)$_3$ as the reference ($\varphi_{PL}$ = 0.73[20] in toluene, $\lambda_{ex}$ = 400 nm); [c] absolute PL quantum yields of the 5 wt% doped film samples (with TCTA as the host ) determined using an integrating sphere at 298 K ($\lambda_{ex}$ = 352 nm); [d] oxidation potential values measured in $CH_2Cl_2$ solutions containing $5\times10^{-4}$ mol $L^{-1}$ of the complexes, referred externally to $Fc/Fc^{+}$; [e] HOMO energy levels deduced from the equation of HOMO = − (4.8 + $E_{1/2}^{ox}$), data in parentheses are those derived from B3LYP calculations; [f] LUMO energy levels obtained from the equation of LUMO = HOMO + $E_g$; [g] $E_g$ estimated from the onset wavelength of the optical absorption bands, data in parentheses derived from B3LYP calculations; [h] decomposition temperature of the complexes (at 5 wt% loss); [i] derived from PL spectra of the 5 wt% doped film samples; [j] Ref.[19].

View Article Online
DOI: 10.1039/C6TC00153J




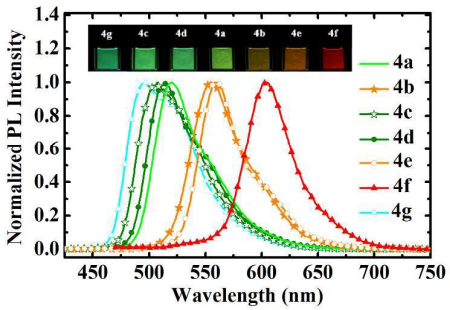


**Figure 2.** Normalized PL emission spectra of **4a**~**4g** in dilute $CH_2Cl_2$ solutions ($\lambda_{ex}$ = 400 nm). The insert is the photograph of **4a**~**4g** under excitation of a UV lamp ($\lambda_{ex}$ = 365 nm).

4,4′,4″-tri(*N*-carbazolyl)triphenylamine (TCTA) with a doping-level of 5wt%, complexes **4b**~**4g** could display moderate $\varphi_{PL}$ of 0.19~0.62. Taking into consideration that the bluish green **4g** shows a relatively high $\varphi_{PL}$ of 1.00 in dilute solution and 0.62 in solid state host, and **4g** is free from fluorine atom that is adverse to the EL performance,[21] it might act as a promising PhOLED material.

### 3.3. Electrochemical properties

The cyclic voltammograms of **4a**~**4g** in dilute $CH_2Cl_2$ solution are shown in Figure 3, and the relevant data are summarized in Table 1. During the anodic scan, all these complexes show a reversible one-electron oxidation wave, which is generally assigned to the $Ir^{IV}/Ir^{III}$ oxidation.[22] The $E^{ox}_{1/2}$ of **4a** is determined to be 0.34 V relative to $Fc/Fc^+$ whose energy level is –4.80 eV in a vacuum,[23] hence the HOMO energy level of **4a** was calculated to be –5.14 eV. For *para*–OMe substituted **4b**, its $E^{ox}_{1/2}$ is 0.21 V lower than that of **4a**, leading to a higher HOMO level of –4.93 eV; while for **4c** bearing a *meta*–OMe, its $E^{ox}_{1/2}$ is just 0.05 eV lower than that of **4a**, hence its HOMO energy level is calculated to be –5.09 eV. Therefore, in both **4b** and **4c**, the –OMe group should act as an EDG arising from its strong electron-donating mesometric effect;[17d] but for $–OCH_3$ group, the *para*-site is a more effective position than the *meta*-site to perturb the HOMO level of the complex. In the cases of the mono–CN substituted **4d** and **4e**, they both display higher $E^{ox}_{1/2}$ hence lower HOMO energy level than that of **4a**, confirming the EWG nature of the –CN group.[24] But the more lowered HOMO level of **4d** than that of **4e** (–5.46 *vs* –5.40 eV) suggests that for –CN substituent, the *para*-site is also a more effective position to influence the HOMO level of the complex. For the di-substituted **4f** and **4g**, their HOMO energy levels are both stabilized compared with that of **4a**. But the HOMO of **4f** (–5.23 eV) lies between that of **4b** and **4e**; and that of **4g** (–5.43 eV) situates just between that of **4c** and **4d**. All these observations validate the presence of synergetic substituent effect of $–OCH_3$ and –CN groups in terms of modulation on the HOMO energy levels of **4f** and **4g**.

Since no reduction wave could be detected in these samples due to the limited range available in $CH_2Cl_2$, the LUMO energy levels of **4a**~**4g** were determined through their HOMO levels and optical bandgaps based on the equation LUMO = HOMO + $E_g$, and the corresponding LUMO energy level of **4a**~**4g** was calculated to be –2.73, –2.68, –2.61, –3.00, –3.12, –3.15, and –2.90 eV in sequence. Accordingly, in comparison with **4a**, both **4b** and **4c** show more destabilized LUMO energy, confirming the EDG nature of $–OCH_3$ group;[17d] while **4d** and **4e** display more stabilized LUMO energy due to the EWG nature of –CN substituent.[24] Moreover, the higher-lying LUMO level of **4c** than **4b** as well as the lower-lying LUMO level of **4e** than **4d** suggest that the *meta*-site is a more effective position than the *para*-one to perturb the LUMO energy level of the chelate.

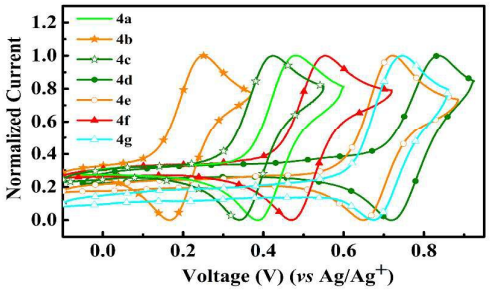


**Figure 3.** Normalized cyclic voltammograms of **4a**~**4g** (measured in $5\times10^{-4}$ mol $L^{-1}$ $CH_2Cl_2$ solution).

Consequently, for complexes bearing a molecular skeleton of **4a**, the *para*- and *meta*-site relative to the Ir atom at the C-ring should be a more effective position to perturb the HOMO and LUMO energy level of the complex, respectively, regardless of the electronic nature of the substituents. As an EDG would generally induce both elevated HOMO and LUMO, but an EWG would often result in lowered HOMO and LUMO,[17d,24] it is reasonable to understand that the grafting of a *meta*–CN or a *para*–$OCH_3$ would induce more lowered LUMO or elevated HOMO level hence red-shifted emission; the introduction of a *para*–CN or a *meta*–$OCH_3$ will result in more lowered HOMO or elevated LUMO level, hence blue-shifted emission; the simultaneous presence of a *meta*–CN or a *para*–$OCH_3$ would endow the complex with both lowered LUMO and elevated HOMO levels, leading to a larger extent of bathochromic shift in emission; while the concurrent existence of a *para*–CN and a *meta*–$OCH_3$ would endow the complex with both lowered HOMO and elevated LUMO levels, hence more blue-shifted emission.

### 3.4. Theoretical calculations

To gain deeper insights into the the origin of the remarkable color-tuning of these complexes induced by merely $–OCH_3$ and –CN substitution on the C-ring, theoretical calculations were performed to optimize the geometry of **4a**~**4g** in their ground state ($S_0$) with B3LYP method of density functional theory. As shown in Table S2, the well-reproduced calculated and experimental structural parameters of **4d**~**4g** confirm the reliability of these calculation results. Based on these optimized $S_0$ structures, the electronic structures as well as the absorption and phosphorescence spectral properties of these compounds in $CH_2Cl_2$ media were investigated (vide Table 1 and S3). The calculated data correspond well with their experimental ones, validating the reliability of our computation results.

As depicted in Figure 4, the HOMO of **4a** is mainly located on the $t_{2g}$-d orbital of the Ir atom (52%) and the π orbitals of phenyl (C-ring) of the C^N ligand (43%); while its LUMO is

View Article Online
DOI: 10.1039/C6TC00153J





primarily distributed on the π* orbitals of the entire C^N ligand (97%) including both the C-ring and N-ring. Hence it is reasonable that the substitution of a –OMe or a –CN group at the C-ring of C^N ligands may perturb the electronic structure of not only the HOMO, but also the LUMO of the complexes. Detailed inspection on the electronic structures of FMOs of **4a** at the C-ring revealed that for the HOMO, the electron density of the C-ring is mainly centered on the *ortho*- and *para*-sites with respect to the iridium atom, but displays nodes at the two *meta*-sites; while the LUMO chiefly resides on the two *meta*-sites relative to the iridium ion, showing nodes at the *ortho*- and *para*-sites (vide Figure 4 and S3). Because a substituent grafted at a position where a MO has significant electron density would generally induce a strong impact on this particular MO, but a group introduced to a position where a MO has a node would bring on only weak influence,[9d,17c,18,25] the substitution on the *para*- or *meta*-site of the C-ring of **4a** should have more influence on the electronic structure of HOMO or LUMO, respectively, which is in line with the electrochemical characterization results. This deduction is further validated from the contours plots of **4b**~**4g** (Figure 4), since in *para*–$OCH_3$ modified (**4b** and **4f**) and *para*–CN substituted (**4d** and **4g**) complexes, substantial π-electron density contribution from –OMe or –CN were observed in their HOMOs; but in *meta*–$OCH_3$ modified (**4c** and **4g**) and *meta*–CN grafted (**4e** and **4f**) compounds, their –OMe or –CN group contributes more effectively to the LUMO.

In accordance with the experimental findings, when being grafted to the C-ring, the –CN group was calculated to induce both lowered HOMO and LUMO levels; while the substitution of a –$OCH_3$ group would often lead to raised HOMO and LUMO levels. Therefore, although the mono-substitution of –$OCH_3$ or –CN at the *para*- or *meta*-sites of the C-ring would induce changes of as large as 0.6 eV in FMO energy levels of the complexes, the changes in $E_g$ of the complexes are just as small as 0.1~0.3 eV, which should be ascribed to the concurrently stabilized or destabilized HOMO and LUMO levels induced by –CN or –OMe substitution.[16d,18,23] Nevertheless, this could be solved through synergetic substituent effect *via* simultaneous substitution of –$OCH_3$ and –CN groups at the C-ring, so that a much enlarged tuning extent of $E_g$ (as large as 0.8 eV) could be achieved.

To further understand the photophysical properties of these chelates, their 20 low-lying $S_0 \rightarrow S_n$ transition energies were calculated based on their $S_0$ geometries, and the simulated absorption spectra of these compounds were shown in Figure S4, the calculated $\lambda_{abs\ max}$ as well as the corresponding transition characters were summarized in Table S3. In line with the experimental findings, the absorption spectra of **4a**~**4g** were all calculated to exhibit two major absorption bands, *i.e.*, a band with $\lambda_{abs\ max}$ of 290~320 nm showing larger transition oscillator strength, and a weaker one with $\lambda_{abs\ max}$ of 380~490 nm stemming from the lowest-lying $S_0 \rightarrow S_1$ transition. For most of these complexes, their stronger absorption band was calculated to be dominated by a LC-featured transition, hence the quite similar absorption character of **4a**~**4g** in the higher-energy region suggest the comparable conjugation length of the C^N ligands in **4a**~**4g**, regardless of the different electronic nature, substitution position and number of their substituents. Note that our results verified that the emission color of Ir(III) complexes is not always correlated with the extent of π-conjugation in their C^N ligands.[8] While the weaker absorption bands of **4a**~**4g** in the lower-energy region were all calculated to be predominated by HOMO→LUMO transition configurations with mixed LC and MLCT character. Consequently, the calculated HOMO-LUMO transition energy gap ($E_g$) of a complex should correlate intimately with its optical bandgap derived from photophysical experiments.

Based on their optimized $S_0$ geometries, the phosphorescence properties of **4a**~**4g** were calculated through their vertical $T_1 \rightarrow S_0$ transition energies. The calculated $T_1 \rightarrow S_0$ energy gaps of most of the complexes correlate well with their experimental $\lambda_{em\ max}$ data (vide Table S3). For **4a**~**4g**, their $T_1 \rightarrow S_0$ deactivation processes were all calculated to be controlled by LUMO→HOMO transition with mixed LC and MLCT transition feature. This accounts for the high correlation between emission energy and $E_g$ data of the chelates, and the structureless phosphorescence bands of these complexes as well.

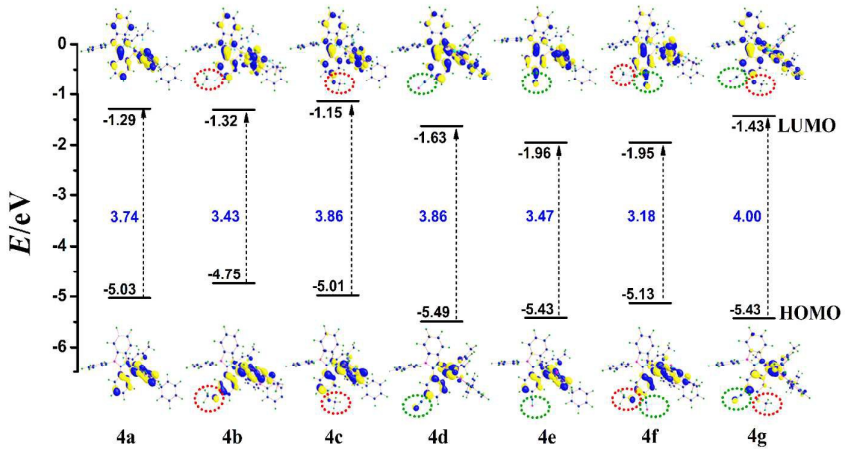


**Figure 4.** Calculated energy level, energy gap and contour plots of HOMO and LUMO of **4a**~**4g** (the –$OCH_3$ and –CN groups are indicated with red and green ellipses, respectively).

View Article Online
DOI: 10.1039/C6TC00153J




All these experimental and calculational results indicated that for Ir(III) complexes whose C-rings of the C^N ligands could contribute substantially to both HOMO and LUMO, their color-tuning direction could be rationally predicted through the electronic nature and the grafting position of $–OCH_3$ and –CN groups at the C-ring. More importantly, the simultaneous grafting of $–OCH_3$ and –CN at positions where both the HOMO and LUMO have significant electron density would lead to a wide shift in the emission energy due to the synergetic substituent effect. Taking into account that the emission color of Ir(III) complexes could be further fine-tuned *via* grafting additional substituents into the C-ring[14a,16a,26-27] or N-ring,[28-29] or the alteration of ancillary ligand,[7] it is reasonable to assume that by grafting a third or fourth substituent at other positions of the C-ring and/or the N-ring where the FMOs have considerable electron density or changing the ancillary ligand, more extended color-tuning ranges could be achieved. In-depth studies on the exploitation of compounds bearing the molecular skeleton of **4a** but showing more red-shifted or blue-shifted emission bands are still carried on, and would be reported elsewhere.

### 3.5. Electroluminescence properties

To evaluate if these objective complexes could act as PhOLED phosphores, their thermal properties were investigated by thermogravimetric analysis (TGA), and their decomposition temperatures were listed in Table 1. All the six objective complexes **4b**-**4g** show relatively high $T_d$ (> 290 °C), indicating that the introduction of –OMe and/or –CN groups into the C-ring of the C^N ligand will not bring adverse effects on the thermostability of the resultant complexes, and all these complexes might be used to fabricate PhOLEDs *via* thermal evaporation process.

Consequently, we chose **4f** or **4g** with the utmost red-shifted or blue-shifted PL emission as the phosphorescent guest dopant, and fabricated PhOLEDs to evaluate if these objective complexes could act as promising EL materials. For **4f**-based Devices $\mathbf{I_a}$~$\mathbf{I_c}$, their device structure is: ITO/TAPC (40 nm)/**4f** (x wt%): TCTA (10 nm)/**4f** (3 wt%): 26DCzPPy (10 nm)/TPBi (40 nm)/LiF (1 nm)/Al (100 nm), where x = 2, 3, 4 in sequence; while for **4g**-based Devices $\mathbf{II_a}$ and $\mathbf{II_b}$, their device structure is ITO/TAPC (40 nm)/**4g** (x wt%): TCTA (10 nm)/**4g** (6 wt%): 26DCzPPy (10 nm)/TmPyPB (40 nm)/LiF (1 nm)/Al (100 nm), where x = 4 and 6 in sequence. Here, ITO acts as the anode; 1,1-bis(4-(*N*,*N*-di(*p*-tolyl)amino)phenyl)cyclohexane (TAPC) acts as the hole-transporting layer; 4,4′,4″-tri(*N*-carbazolyl)triphenylamine (TCTA) and 2,6-bis(3-(9*H*-carbazol-9-yl)phenyl)pyridine (26DCzPPy) act as the host materials for **4f** and **4g** with hole- and electron-transporting capability, respectively; 1,3,5-tris(*N*-phenylbenzimidazol-2-yl)benzene (TPBi) or 1,3,5-tri(*m*-pyrid-3-yl-phenyl)benzene (TmPyPB) acts as the electron-transporting layer; LiF/Al acts as the cathode. The energy level alignment of these devices was shown in Figure 5.

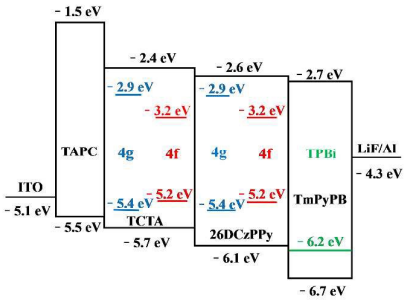


**Figure 5.** Device configuration and energy band diagram of Devices $\mathbf{I_a}$~$\mathbf{I_c}$ and $\mathbf{II_a}$~$\mathbf{II_b}$.

As shown in Figure 6 and Figure S5, the **4f**-based Devices $\mathbf{I_a}$~$\mathbf{I_c}$ could emit bright red EL with $\lambda_{EL\ max}$ of 600 nm; while **4g**-based Devices $\mathbf{II_a}$ and $\mathbf{II_b}$ display intense bluish green EL with $\lambda_{EL\ max}$ of 496~499 nm. In all the five devices, the electrophosphorescence bands exactly resemble the PL spectra of complexes **4f** or **4g** in dilute $CH_2Cl_2$ solution (vide Figure 2), implying the EL emission mainly originates from the radiative decay of **4f** or **4g**. It should be pointed out that in the EL spectra of Devices $\mathbf{I_a}$~$\mathbf{I_c}$, the emission of the host compounds peaked at ~390 nm (TCTA and/or 26DCzPPy) is also discernible. This may be ascribed to the unfavorable energy level alignment in $\mathbf{I_a}$~$\mathbf{I_c}$ and the relatively low energy transfer efficiency between the **4f** and the host material (vide Figure S6).[30]

As shown in Table 2, Figure 7 and Figure S7~S8, all these five devices show relatively low turn-on voltage (< 3.5 V). For the **4f**-based red Devices $\mathbf{I_a}$~$\mathbf{I_c}$, $\mathbf{I_b}$ with a doping-level of 3 wt% shows the best performance, with maximum brightness ($L_{max}$), current efficiency ($LE_{max}$), external quantum efficiency ($EQE_{max}$) and power efficiency ($PE_{max}$) of 18260 cd $m^{-2}$, 10.4 cd $A^{-1}$, 4.5% and 9.5 lm $W^{-1}$, respectively; while for the two bluish green **4g**-based devices, $\mathbf{II_b}$ shows better performance, with $L_{max}$ of 48040 cd $m^{-2}$, $LE_{max}$ of 62.1 cd $A^{-1}$, $EQE_{max}$ of 19.8% and $PE_{max}$ of 42.2 lm $W^{-1}$. It is noteworthy that in all the devices, satisfactory current efficiency could be achieved at high brightness. For Device $\mathbf{I_b}$, its LE maintains to be as high as 7.8 cd $A^{-1}$ at 1000 cd $m^{-2}$, 6.9 cd $A^{-1}$ at 2000 cd $m^{-2}$, and 5.3 cd $A^{-1}$ at 5000 cd $m^{-2}$. In the case of Device $\mathbf{II_b}$, its $LE_{max}$ was even obtained under a relatively high luminance of >1000 cd

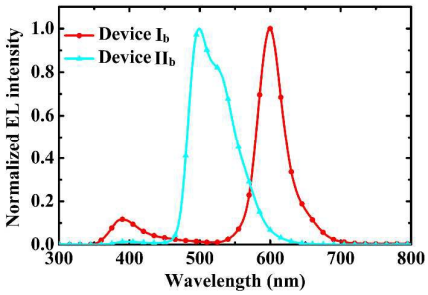


**Figure 6.** EL spectra of Devices $\mathbf{I_b}$ and $\mathbf{II_b}$ (driving current density: 1 mA $cm^{-2}$).

View Article Online
DOI: 10.1039/C6TC00153J



**Table 2.** EL performance of Devices $\mathbf{I_a}$~$\mathbf{I_c}$ and $\mathbf{II_a}$~$\mathbf{II_b}$.

| Device | Dopant | Dopting level [wt %] | $\lambda_{EL\ max}$ (nm) | $V_{on}$ [a] (V) | $L_{max}$ [b] (cd m$^{-2}$) | $LE_{max}$ [c] (cd A$^{-1}$) | $PE_{max}$ [d] (lm W$^{-1}$) | $EQE_{max}$ (%) | CIE (x, y) |
|---|---|---|---|---|---|---|---|---|---|
| $\mathbf{I_a}$ | **4f** | 2 | 600 | 3.3 | 13070 | 8.0 | 5.8 | 3.5 | (0.57,0.37) |
| $\mathbf{I_b}$ | **4f** | 3 | 600 | 3.4 | 18260 | 10.4 | 9.5 | 4.5 | (0.57,0.38) |
| $\mathbf{I_c}$ | **4f** | 4 | 600 | 3.4 | 16980 | 8.9 | 7.0 | 3.8 | (0.58,0.39) |
| $\mathbf{II_a}$ | **4g** | 4 | 496 | 3.0 | 31850 | 41.9 | 22.3 | 14.1 | (0.20,0.57) |
| $\mathbf{II_b}$ | **4g** | 6 | 499 | 3.2 | 48040 | 62.1 | 42.2 | 19.8 | (0.22,0.58) |

[a] Turn-on voltage at 1 cd m$^{-2}$; [b] maximum luminance; [c] maximum current efficiency; [d] maximum power efficiency.

m$^{-2}$, and the LE of this device maintains to be 61.9 cd A$^{-1}$ at 2000 cd m$^{-2}$, 58.2 cd A$^{-1}$ at 5000 cd m$^{-2}$, and 50.3 cd A$^{-1}$ at 10000 cd m$^{-2}$. In comparison with Devices **II**, the red Devices **I** display much inferior EL performance, which should be ascribed to the unmatched energy levels between host and guest compounds, and the relatively low photoluminescence quantum yield of compound **4f** as well. Nevertheless, although the performance of these two devices is still inferior to that of the state-of-art red and bluish green PhOLEDs, much improved EL performance could be expected after further optimization has been carried out on the host species, device structure, doping concentration as well as layer thickness.

All these preliminary EL characterization results indicated that through this simple but effective –CN and/or –OMe subsitution strategy on the C-ring of the C^N ligand, the resulted Ir(III) complexes could not only display a wide color-tuning range, but also act as quite promising EL materials. Therefore, this facile color-modulating strategy is quite effective in developing high-performance red and blue PhOLED iridium complexes.

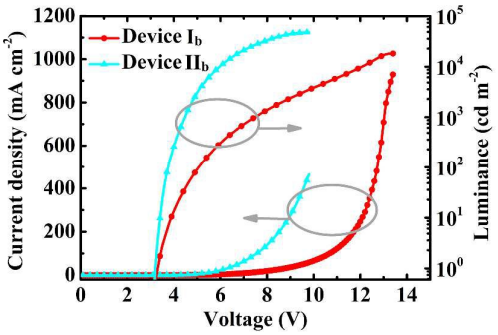


**Figure 7.** Current density–voltage–luminance (*J–V–L*) characteristics of Devices $\mathbf{I_b}$ and $\mathbf{II_b}$.

## Conclusions

In this work, we developed a novel facile strategy for rational fine-tuning of phosphorescence color of Ir(III) complexes, *i.e.*, utilizing the synergetic substituent effect of methoxy and cyano groups at only the C-ring of the C^N ligand to modulate the FMO energy level hence the bandgap of the complexes. Based on experimental and theoretical studies, the following structure-properties relationship of Ir(III) complexes has been deciphered: 1) for **4a**-based Ir(III) complexes, the introduction of a –OMe or a –CN to the C-ring of the C^N ligand would usually endow them with raised or lowered FMO energy levels, respectively, regardless of the substitution position (*para*- or *meta*-site with respect to the Ir atom); 2) for both –OMe and –CN groups, the *para*-site of the C-ring is a more effective substitution position to modulate the HOMO energy levels due to the fact that the electronic densities of HOMO are mainly located at the position, but the *meta*-site would induce a stronger impact on the LUMO energy levels because the electronic densities of LUMO mainly reside on this site; 3) the –OMe and –CN groups on *para*- or *meta*-site of the C-ring could display a synergetic effect with regard to the fine-tune of FMO energy levels, leading to a wide shift in the emission energy.

Using this simple strategy, a library of Ir(III) complexes whose emission-color nearly covers the whole visible region has been developed. Our results show the efficacy of this color-tuning strategy through substitution merely on the C-ring of C^N ligands where both HOMO and LUMO show significant electron density, and the broader ramification of this study lies in the rational molecular design of Ir(III) complexes with desirable phosphorescence color, which are expected to fill an urgent need for high-performance Ir(III) complexes for diverse optoelectronic applications.

## Acknowledgements

We acknowledge the financial support for this work by the National Natural Science Foundation of China (project No. 21372168, 21432005, U1230121, 21190031 and 21201161), Youth Innovation Promotion Association CAS (2013150), Sichuan Province Science and Technology Support Program (2015GZ0193), and Jilin Provincial Science and Technology Development Program of China (20130522125JH). We are grateful to the Analytical & Testing Centre of Sichuan University and Comprehensive Training Platform of Specialized Laboratory, College of Chemistry, Sichuan University for providing NMR, HR-MS and single crystal X-ray diffraction data for the intermediates and objective molecules.

## Notes and references

1 (a) X. Yang, G. Zhou and W. Y. Wong, *Chem. Soc. Rev.*, 2015, **44**, 8484–8575; (b) H. Sasabe, H. Nakanishi, Y. Watanabe, S. Yano, M. Hirasawa, Y. J. Pu and J. Kido, *Adv. Funct. Mater.*, 2013, **23**, 5550–5555; (c) Y. H. Lee, J. Park, J.

View Article Online
DOI: 10.1039/C6TC00153J


Lee, S. U. Lee and M. H. Lee, *J. Am. Chem. Soc*., 2015, **137**, 8018–8021; (d) R. Wang, L. Deng, T. Zhang and J. Li, *Dalton Trans*., 2012, **41**, 6833–6841; (e) C. Fan, L. Zhu, B. Jiang, Y. Li, F. Zhao, D. Ma, J. Qin and C. Yang, *J. Phys. Chem. C.,* 2013, **117**, 19134–19141; (f) W. Y. Wong and C. L. Ho, *J. Mater. Chem*., 2009, **19**, 4457–4482; (g) W. Y. Wong and C. L. Ho, *Coord. Chem. Rev.,* 2009, **253**, 1709–1758; (h) L. Ying, C. L. Ho, H. Wu, Y. Cao and W. Y. Wong, *Adv. Mater*., 2014, **26**, 2459–2473.

2 K. H. Kim, C. K. Moon, J. H. Lee, S. Y. Kim and J. J. Kim, *Adv. Mater*., 2014, **26**, 3844–3847.

3 (a) C. H. Fan, P. Sun, T. H. Su and C. H. Cheng, *Adv. Mater*., 2011, **23**, 2981–2985; (b) C. L. Ho, H. Li and W. Y. Wong, *J. Organomet. Chem*., 2014, **751**, 261–285.

4 (a) M. Kim and J. Y. Lee, *Adv. Funct. Mater*., 2014, **24**, 4164–4169; (b) J. Lee, H. F. Chen, T. Batagoda, C. Coburn, P. I. Djurovich, M. E. Thompson and S. R. Forrest, *Nat. Mater*., 2015, **15**, 92–98; (c) S. Gong, N. Sun, J. Luo, C. Zhong, D. Ma, J. Qin and C. Yang, *Adv. Funct. Mater.*, 2014, **24**, 5710–5718; (d) C. L. Ho and W. Y. Wong, *New J. Chem.,* 2013, **37**, 1665–1683.

5 For selected reviews, see (a) C. Fan and C. Yang, *Chem. Soc. Rev*., 2014, **43**, 6439–6469; (b) T. Tsuboi and W. Huang, *Isr. J. Chem*., 2014, **54**, 885–896; (c) G. Zhou, W. Y. Wong and S. Suo, *J. Photochem. Photobiol., C: Photochem. Rev.* 2010, **11**, 133–156; (d) G. Zhou, W. Y. Wong and X. Yang, *Chem. – Asian J.,* 2011, **6**, 1706–1727; (e) X. Yang, G. Zhou and W. Y. Wong, *J. Mater. Chem. C*, 2014, **2**, 1760–1778.

6 (a) S. Lamansky, P. Djurovich, D. Murphy, F. Abdel-Razzaq, H.-E. Lee, C. Adachi, P. E. Burrows, S. R. Forrest and M. E. Thompson, *J. Am. Chem. Soc*., 2001, **123**, 4304–4312; (b) Y. Zhou, H. Gao, X. Wang and H. Qi, *Inorg. Chem*., 2015, **54**, 1446–1453; (c) J. Li, R. Wang, R. Yang, W. Zhou and X. Wang, *J. Mater. Chem. C,* 2013, **1**, 4171–4179.

7 (a) Y. You and S. Y. Park, *J. Am. Chem. Soc*., 2005, **127**, 12438–12439; (b) K. Y. Lu, H. H. Chou, C. H. Hsieh, Y. H. O. Yang, H. R. Tsai, H. Y. Tsai, L. C. Hsu, C. Y. Chen, I. Chen and C. H. Cheng, *Adv. Mater*., 2011, **23**, 4933–4937.

8 (a) L.-L. Wu, S.-H. Tsai, T.-F. Guo, C.-H. Yang and I.-W. Sun, *J. Lumin*., 2007, **126**, 687–694; (b) A. Bossi, A. F. Rausch, M. J. Leitl, R. Czerwieniec, M. T. Whited, P. I. Djurovich, H. Yersin and M. E. Thompson, *Inorg. Chem*., 2013, **52**, 12403−12415; (c) Li.-M. Xie, F.-Q. Bai, W. Li, Zh.-X. Zhang and H.-X. Zhang, *Phys. Chem. Chem. Phys.*, 2015, **17**, 10014−10021.

9 (a) V. V. Grushin, N. Herron, D. D. LeCloux, W. J. Marshall, V. A. Petrov and Y. Wang, *Chem. Commun*., 2001, **16**, 1494−1495; (b) T. Tsuzuki, N. Shirasawa, T. Suzuki and S. Tokito, *Adv. Mater*., 2003, **15**, 1455−1458; (c) G. Zhou, C. L. Ho, W. Y. Wong, Q. Wang, D. Ma, L. Wang, Z. Lin, T. B. Marder and A. Beeby, *Adv. Funct. Mater*., 2008, **18**, 499−511; (d) D. Wang, Y. Wu, B. Jiao, G. Zhou, G. Wang and Z. Wu, *Org. Electron*., 2013, **14**, 2233−2242.

10 (a) S. Yang, J. You, J. Lan and G. Gao, *J. Am. Chem. Soc*., 2012, **134**, 11868−11871; (b) Y. Wang, J. Zhou, X. Wang, X. Zheng, Z. Lu, W. Zhang, Y. Chen, Y. Huang, X. Pu and J. Yu, *Dyes Pigments*, 2014, **100**, 87−96.

11 (a) R. F. Wissner, S. Batjargal, C. M. Fadzen and E. J. Petersson, *J. Am. Chem. Soc*., 2013, **135**, 6529−6540; (b) H. Kim, C. Y. W. Ng and W. R. Algar, *Langmuir*, 2014, **30**, 5676−5685; (c) E. Lee, C. Kim and J. Jang, *Chem. – Eur. J*., 2013, **19**, 10280–10286.

12 M. A. Baldo, M. E. Thompson and S. R. Forrest, *Nature*, 2000, **403**, 750–753.

13 P. J. Hay, *J. Phys. Chem. A*., 2002, **106**, 1634–1641.

14 (a) S.-y. Takizawa, J.-i. Nishida, T. Tsuzuki, S. Tokito and Y. Yamashita, *Inorg. Chem*., 2007, **46**, 4308–4319; (b) J.-i. Nishida, H. Echizen, T. Iwata and Y. Yamashita, *Chem. Lett*., 2005, **34**, 1378–1379; (c) T.-H. Kwon, H. S. Cho, M. K. Kim, J.-W. Kim, J.-J. Kim, K. H. Lee, S. J. Park, I.-S. Shin, H. Kim and D. M. Shin, *Organometallics*, 2005, **24**, 1578–1585; (d) C.-H. Yang, S.-W. Li, Y. Chi, Y.-M. Cheng, Y.-S. Yeh, P.-T. Chou, G.-H. Lee, C.-H. Wang and C.-F. Shu, *Inorg. Chem*., 2005, **44**, 7770–7780.

15 W. Mróz, R. Ragni, F. Galeotti, E. Mesto, C. Botta, L. De Cola, G. M. Farinola and U. Giovanella, *J. Mater. Chem. C*, 2015, **3**, 7506–7512.

16 (a) Q.-L. Xu, C.-C. Wang, T.-Y. Li, M.-Y. Teng, S. Zhang, Y.-M. Jing, X. Yang, W.-N. Li, C. Lin and Y.-X. Zheng, *Inorg. Chem*., 2013, **52**, 4916–4925; (b) T. Kim, H. Kim, K. M. Lee, Y. S. Lee and M. H. Lee, *Inorg. Chem*., 2013, **52**, 160–168; (c) R. Ragni, E. Orselli, G. S. Kottas, O. H. Omar, F. Babudri, A. Pedone, F. Naso, G. M. Farinola and L. De Cola, *Chem. – Eur. J*., 2009, **15**, 136–148; (d) X. Yang, N. Sun, J. Dang, Z. Huang, C. Yao, X. Xu, C.-L. Ho, G. Zhou, D. Ma, X. Zhao and W. Y. Wong, *J. Mater. Chem. C*, 2013, **1**, 3317–3326.

17 (a) I. R. Laskar and T.-M. Chen, *Chem. Mater*., 2004, **16**, 111–117; (b) W.-C. Chang, A. T. Hu, J.-P. Duan, D. K. Rayabarapu and C.-H. Cheng, *J. Organomet. Chem*., 2004, **689**, 4882–4888; (c) S. Jung, Y. Kang, H. S. Kim, Y. H. Kim, C. L. Lee, J. J. Kim, S. K. Lee and S. K. Kwon, *Eur. J. Inorg. Chem*., 2004, 3415–3423; (d) K. Hasan, A. K. Bansal, I. D. W. Samuel, C. Roldán-Carmona, H. J. Bolink and E. Zysman-Colman, *Sci. Rep*., 2015, **5**, 12325; (e) J. Frey, B. F. E. Curchod, R. Scopelliti, I. Tavernelli, U. Rothlisberger, M. K. Nazeeruddin and E. Baranoff, *Dalton Trans*., 2014, **43**, 5667–5679.

18 I. Avilov, P. Minoofar, J. Cornil and L. De Cola, *J. Am. Chem. Soc*., 2007, **129**, 8247–8258.

19 (a) W.-S. Huang, J. T. Lin, C.-H. Chien, Y.-T. Tao, S.-S. Sun and Y.-S. Wen, *Chem. Mater*., 2004, **16**, 2480–2488; (b) W.-S. Huang, J. T. Lin and H.-C. Lin, *Org. Electron*., 2008, **9**, 557–568.

20 W. Holzer, A. Penzkofer and T. Tsuboi, *Chem. Phys*., 2005, **308**, 93–102.

21 (a) D. Tordera, J. J. Serrano-Pérez, A. Pertegás, E. Ortí, H. J. Bolink, E. Baranoff, M. K. Nazeeruddin and J. Frey, *Chem. Mater*., 2013, **25**, 3391–3397; (b) C.-H. Lin, Y.-Y. Chang, J.-Y. Hung, C.-Y. Lin, Y. Chi, M.-W. Chung, C.-L. Lin, P.-T. Chou, G.-H. Lee, C.-H. Chang and W.-C. Lin, *Angew. Chem*., *Int. Ed*., 2011, **50**, 3182–3286.

22 K. R. J. Thomas, M. Velusamy, J. T. Lin, C.-H. Chien, Y.-T. Tao, Y. S. Wen, Y.-H. Hu and P.-T. Chou, *Inorg. Chem*., 2005, **44**, 5677–5685.

23 L. Chen, C. Yang, J. Qin, J. Gao and D. Ma, *Inorg. Chim. Acta*, 2006, **359**, 4207–4214.

24 Y. Si, X. Sun, Y. Liu, X. Qu, Y. Wang and Z. Wu, *Dalton Trans*., 2014, **43**, 714–721.

25 W. Fan, X. Sun, G. Zhu, Y. Guo, Z. Si and C. Wang, *Synth. Met*., 2012, **162**, 1190–1197.

26 (a) S. Aoki, Y. Matsuo, S. Ogura, H. Ohwada, Y. Hisamatsu, S. Moromizato, M. Shiro and M. Kitamura, *Inorg. Chem*., 2011, **50**, 806–818; (b) Y. Hisamatsu and S. Aoki, *Eur. J. Inorg. Chem*., 2011, 5360–5369.

27 (a) C. Fan, Y. Li, C. Yang, H. Wu, J. Qin and Y. Cao, *Chem. Mater*., 2012, **24**, 4581–4587; (b) Y. Wang, N. Sun, B. F. E. Curchod, L. Male, D. Ma, J. Fan, Y. Liu, W. Zhu and E. Baranoff, *J. Mater. Chem. C*, 2015, DOI: 10.1039/c5tc02355f.

28 (a) D. D. Censo, S. Fantacci, F. D. Angelis, C. Klein, N. Evans, K. Kalyanasundaram, H. J. Bolink, M. Gratzel and M. K. Nazeeruddin, *Inorg. Chem*., 2008, **47**, 980–989; (b) M. Xu, R. Zhou, G. Wang and J. Yu, *Inorg. Chim. Acta*, 2009, **362**, 2183–2188.

View Article Online
DOI: 10.1039/C6TC00153J



29 (a) H. Jang, C. H. Shin, N. G. Kim, K. Y. Hwang and Y. Do, *Synth. Met.*, 2005, **154**, 157–160; (b) S.-y. Takizawa, H. Echizen, J.-i. Nishida, T. Tsuzuki, S. Tokito and Y. Yamashita, *Chem. Lett.*, 2006, **35**, 748–749; (c) K. S. Bejoymohandas, A. Kumar, S. Varughese, E. Varathan, V. Subramanian and M. L. P. Reddy, *J. Mater. Chem. C*, 2015, **3**, 7405–7420.

30 (a) D. Wasserberg, S. C. J. Meskers and R. A. J. Janssen, *J. Phys. Chem. A.*, 2007, **111**, 1381–1388; (b) H. Fukagawa, T. Shimizu, H. Hanashima, Y. Osada, M. Suzuki and H. Fujikake, *Adv. Mater.*, 2012, **24**, 5099–5103.

View Article Online
DOI: 10.1039/C6TC00153J



## Graphical Abstract

A facile color-tuning strategy for constructing a library of Ir(III) complexes with fine-tuned phosphorescence from bluish green to red using synergetic substituent effect of $-OCH_3$ and –CN at merely the C-ring of C^N ligand

Yan Jiao,‡[a] Ming Li,‡[a] Ning Wang,[a] Tao Lu,[a] Liang Zhou,*[b] Yan Huang,[a] Zhiyun Lu,*[a] Daibing Luo[c] and Xuemei Pu*[a]

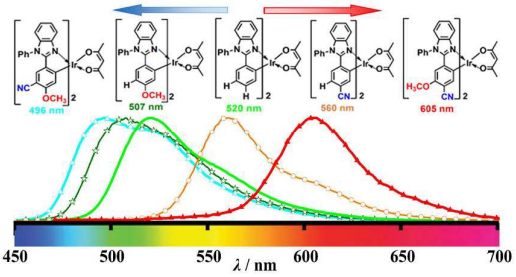


$-OCH_3$ and –CN will show a favorable synergetic substituent effect on the color-tuning direction when they are grafted at the *meta*- and *para*-sites of the C-ring of the C^N ligand.